Published OnlineFirst July 12, 2021; DOI: 10.1158/1535-7163.MCT-20-1097



# Valency of HER2 Targeting Antibodies Influences Tumor Cell Internalization and Penetration

Madeleine K. Ramos, Danielle Mandikian, Lauren N. Sermeño, Anna King, Alecia T. Dent, Jason Ho, Sheila Ulufatu, T. Noelle Lombana, Christoph Spiess, Mary Ann T. Go, Shang-Fan Yu, Amrita V. Kamath, Gregory Z. Ferl, and C. Andrew Boswell

## ABSTRACT

T-cell–dependent bispecific antibodies (TDB) have been a major advancement in the treatment of cancer, allowing for improved targeting and efficacy for large molecule therapeutics. TDBs are comprised of one arm targeting a surface antigen on a cancer cell and another targeting an engaging surface antigen on a cytotoxic T cell. To impart this function, the antibody must be in a bispecific format as opposed to the more conventional bivalent format. Through *in vitro* and *in vivo* studies, we sought to determine the impact of changing antibody valency on solid tumor distribution and catabolism. A bivalent anti-HER2 antibody exhibited higher catabolism than its full-length monovalent binding counterpart *in vivo* by both invasive tissue harvesting and noninvasive single photon emission computed tomography/X-ray computed tomography imaging despite similar systemic exposures for the two molecules. To determine what molecular factors drove *in vivo* distribution and uptake, we developed a mechanistic model for binding and catabolism of monovalent and bivalent HER2 antibodies in KPL4 cells. This model suggests that observed differences in cellular uptake of monovalent and bivalent antibodies are caused by the change in apparent affinity conferred by avidity as well as differences in internalization and degradation rates of receptor bound antibodies. To our knowledge, this is the first study to directly compare the targeting abilities of monovalent and bivalent full-length antibodies. These findings may inform diverse antibody therapeutic modalities, including T-cell–redirecting therapies and drug delivery strategies relying upon receptor internalization.

## Introduction

Bispecific antibodies recognize and bind two different epitopes. The ability to bridge two specific target ligands via a therapeutic molecule, or to target two interacting biological pathways are mechanisms by which bispecific antibodies are able to provide increased functionality over existing monospecific molecule therapeutics (1, 2). One class of bispecific molecules showing promise in oncology are T-cell–dependent bispecific antibodies (TDB). These bispecific antibodies target surface antigens on both cancer cells and T cells which form an artificial immunologic synapse (3), resulting in selective killing of target-expressing tumor cells (4). Multiple formats of TDBs have shown increased efficacy and potent selective cell killing over existing therapies in both preclinical and clinical hematologic cancer studies (5, 6). For solid tumors, potent antitumor activity has been observed in multiple preclinical models with an anti-HER2/CD3 full-length TDB (7), which is currently being evaluated in a phase I clinical trial (8).

However, one question that has not been fully explored is how the monovalent format of TDBs affects tumor distribution and cellular uptake. Incomplete solid tumor penetration have been observed with a number of anticancer therapeutics including trastuzumab (9, 10). One characteristic that must be considered is valency, or the number of target binding sites on a molecule. An increase in valency from monovalent to bivalent would increase the apparent affinity, conferred by avidity, of an antibody as long as each site can freely bind its cell surface target. Therefore, changes in valency could affect the pattern of distribution, and significantly influence efficacy. Beyond the potential relevance for design of TDBs, understanding the impact of valency for a given target on distribution may have broader application to other bispecific antibodies such as those designed to enhance antibody uptake in difficult to access tissues (11). We investigated how valency, and therefore apparent affinity, affects the *in vivo* distribution and uptake of HER2-targeting antibodies in solid tumors.

## Materials and Methods

### Production of antibodies

The anti-HER2 antibody is hu4D5-8, generated as described previously (12). To control for tissue/tumor uptake in the absence of target binding, we employed a targeting arm recognizing viral glycoprotein D (gD). The bivalent anti-gD and anti-HER2 antibodies were expressed in CHO cells. The bispecific antibody (anti-gD/HER2) was generated using the knobs-into-holes strategy (13, 14) by half-antibodies expressed in CHO cells and assembled as described previously (7).

### Radiochemistry

Iodine-125 ($^{125}$I) was obtained as sodium iodide from Perkin Elmer. $^{125}$I was used to iodinate at a specific activity of ~10 μCi/μg using the indirect Iodogen method (Pierce Chemical Co.). Radiosynthesis of $^{111}$In labeled antibodies (~6 μCi/μg) was achieved though chelation of $^{111}InCl_3$ into 1,4,7,10-tetraazacyclododecane-1,4,7,10-tetraacetic acid (DOTA)-conjugated mAbs. Purification of all radioimmunoconjugates was achieved using NAP5 columns and confirmed by radio-size-exclusion chomatography.

Genentech, Inc., One DNA Way, South San Francisco, California.

**Note:** Supplementary data for this article are available at Molecular Cancer Therapeutics Online (http://mct.aacrjournals.org/).

M.K. Ramos, D. Mandikian, G.Z. Ferl, and C. Andrew Boswell contributed equally to this article.

**Corresponding Authors:** C. Andrew Boswell, Preclinical and Translational Pharmacokinetics, Genentech, Inc., 1 DNA Way, MS 463A, South San Francisco, CA 94080. E-mail: boswell.andy@gene.com; and Gregory Z. Ferl, ferl.gregory@gene.com

Mol Cancer Ther 2021;20:1956–65

**doi:** 10.1158/1535-7163.MCT-20-1097

Published OnlineFirst July 12, 2021; DOI: 10.1158/1535-7163.MCT-20-1097



### *In vivo* tissue distribution studies

All animal studies were conducted in accordance with the guidelines and with approval of the American Association for Accreditation of Laboratory Animal Care and the Genentech Institutional Animal Care and Use Committee (IACUC). The HER2-expressing (IHC 3+) human breast cancer cell line KPL-4 was used for both *in vivo* and *in vitro* studies. Female C.B-17 SCID.bg adult mice (Charles River Laboratories; 6–8 weeks and 20–25 g) were inoculated in the right mammary fat pad with ∼3 million KPL-4 cells in a 50:50 suspension of HBSS (Invitrogen) and Matrigel (BD Biosciences). Mice were randomly assigned into groups ($n = 4$ per group) when mean tumor volumes reached 300 to 400 $mm^3$.

To minimize thyroid sequestration of $^{125}I$, all mice received an intraperitoneal injection of 100 μL of 30 mg/mL of sodium iodide at 1 and 24 hours before receiving radiolabeled antibodies. All mice received a single intravenous bolus via the tail vein containing $^{125}I$- and $^{111}In$-labeled antibodies (5 μCi each) together with the respective unmodified antibody for a total dose of 1 or 10 mg/kg (anti-gD/HER2), 0.5 or 5 mg/kg (anti-HER2/HER2), or 5 mg/kg (anti-gD/gD), to dose normalize by targeting arm molarity.

Mice were bled over the course of the study to derive plasma and whole blood antibody concentrations. Mice were sacrificed at 6 hours, 1 day, and 7 days for tissue distribution, except for the control group (anti-gD/gD), which was only harvested at 7 days. On each harvest, tissue samples were terminally collected, rinsed with PBS, blotted dry, and weighed. Tumors were collected for further processing for microscopy experiments. All tissues were counted using a 2480 Wizard2 automatic gamma counter (Perkin Elmer). Counts per minute of harvested tissues and input dosing solution were used to calculate the percentage of injected dose per gram of tissue [% ID/g = (tissue CPM/input dosing solution CPM *100%)/tissue weight]. The dual radiotracer tracer approach ($^{125}I$ and $^{111}In$) distinguishes intact from catabolized antibodies (15). Intact antibodies were determined from the measurement of $^{125}I$, whereas the amount of catabolized antibody was estimated as the $^{111}In$-labeled antibody %ID/g (Intact + Catabolized) minus $^{125}I$-labeled antibody %ID/g (Intact).

### Single-photon emission computed tomography/X-ray computed tomography imaging

Noninvasive *in vivo* distribution was obtained by single-photon emission computed tomography/X-ray computed tomography (SPECT-CT) using a modification of previously reported methods (MiLabs; ref. 4). Radiolabeling procedures and tumor generation were identical as for the biodistribution study. Imaging mice received a single dose containing $^{125}I$-labeled (5 μCi) and $^{111}In$-labeled antibodies (700 μCi, imaging relevant dose) together with the respective unmodified antibody for a total dose of 10 mg/kg (anti-gD/HER2, $n = 2$), 5 mg/kg (anti-HER2/HER2, $n = 1$), or 5 mg/kg (anti-gD/gD, $n = 1$). Mice were imaged at 6 hours, 1 day, 2 days, 3 days, and 7 days after dose. Immediately following CT acquisition, SPECT images were acquired in two 20% windows centered at the 173- and 247-keV photopeaks of $^{111}In$ using the Extra Ultra-High Sensitivity Mouse collimator with a 2 mm pinhole and reconstructed resolution of ∼0.85 $mm^3$. SPECT data were acquired using spiral mode exposures for 20 minutes. Terminally collected tumors were scanned using the Exirad collimator with a 0.15 mm pinhole and a reconstructed resolution of ∼0.25 $mm^3$. Tumors were processed and analyzed as in the invasive biodistribution study. SPECT image analysis and quantification was accomplished using VivoQuant (Invicro).

### Microscopy

After gamma counting, all tumors from the biodistribution study were drop-fixed in 4% paraformaldehyde overnight at 4°C. The tumors were washed in PBS and cryoprotected in sucrose. Frozen tumors were embedded in block with Richard-Allan Scientific Neg-50 Frozen Section Medium (Thermo Fisher Scientific) and sectioned on a CryoStar NX70 Cryostat (Thermo Fisher Scientific) at 5 μm from the center of each tumor.

Tumor sections were washed in 0.1 mol/L phosphate buffer (PB) and blocked/permeabilized (10% normal goat serum/0.1% Triton-X/0.1 mol/L PB) for 1 hour at room temperature. Sections were incubated with Rabbit anti-Human IgG (H+L) (1.2 μg/mL) overnight at 4°C. Sections were then incubated with Goat anti-Rabbit IgG (H+L) Alexa Fluor-680 (1 μg/mL) overnight at 4°C. Coverslips were mounted with ProLong Gold Antifade with DAPI (Thermo Fisher Scientific).

Fluorescently labeled slides were imaged with a 20×/0.8 Plan-Apochromat objective on an Axio Scan.Z1 (Zeiss) using the same exposure times. Images were exported as TIFFs using Zen (Zeiss) and image montages were generated using Photoshop (Adobe) where all signals were linearly increased together.

### Data and statistical analysis

All values are expressed as mean ± SD, and $P$ values were assessed by unpaired, two-tailed, Student $t$ test, unless otherwise indicated. $P < 0.05$ was considered statistically significant. Comprehensive statistics are reported in Supplementary Table S2.

### *In vitro* binding and uptake assays

A total of 60,000 KPL-4 cells were plated per well in 24-well plates. Media was replaced with fresh media spiked with a mixture of $^{125}I$- and $^{111}In$-labeled anti-gD/gD, anti-gD/HER2 and anti-HER2/HER2 antibodies at 0.25 μCi (∼0.08 μg antibody, $\sim 3.2_E{}^{11}$ antibodies/well) of each respective antibody per well and incubated at 37°C. At each time point, four replicate wells were washed three times with warm Hank's Balanced Salt Solution (HBSS) and harvested following incubation with trypsin for 15 minutes at 37°C. Inputs (radiolabeled-antibody spiked media) as well as harvested cells were counted using a gamma counter as described above. Counts per minute of harvested cells and input media were used to calculate the percentage of plated antibody (% AP = harvested cell CPM/media input CPM × 100%) bound to and accumulated within the cells.

### Compartmental modeling of *in vitro* binding and uptake data

Uptake and residualization kinetics of the monovalent and bivalent antibodies in KPL4 cells were analyzed using a compartmental modeling approach based on previously published compartmental models of anti-HER2 antibody trafficking (16, 17). The key mechanisms captured include basal rates of HER2 synthesis, recycling and degradation, anti-HER2 antibody binding and dissociation at the cell surface and within endosomes, degradation of free and unbound internalized antibodies, and residualization of the radiolabeled linker/amino acid fragment $^{111}In$-DOTA-Lys (**Table 1**).

Although only a single-model structure is considered in this analysis, several model parameterization variants are evaluated to investigate conflicting views existing in the literature regarding the fate of HER2 upon binding by anti-HER2 antibodies. Some reports claim that HER2 is passive and unaffected by anti-HER2 binding (18) whereas others claim that internalization is induced upon antibody binding, presumably via cross-linking of HER2 homodimers by the antibody (16). Nevertheless, if the rate or extent of HER2 internalization is enhanced by anti-HER2 antibody binding,

Published OnlineFirst July 12, 2021; DOI: 10.1158/1535-7163.MCT-20-1097



**Table 1.** Fitted parameter values for Model Variant 4.

| | Parameter | Units | Description | Value |
|---|---|---|---|---|
| Fitted parameters | $t_{1/2,\ int}^{HER2}$ | hour | Internalization half-life of unbound and monovalent mAb-bound HER2 | 10 |
| | $t_{1/2,deg}^{HER2}$ | hour | Degradation half-life of unbound and monovalent mAb-bound HER2 | 23 |
| | $K_D^{mono}$ | nmol/L | Equilibrium dissociation constant of monovalent mAb | 4.4 |
| | $K_D^{bival}$ | nmol/L | Equilibrium dissociation constant of bivalent mAb | 0.64 |
| | $t_{1/2}^{delay}$ | hour | Time delay between late endosome/lysosome and residualized $^{111}$In-mAb compartments | 7.7 |
| | $k_{off}^{mono}$ | 1/hour | First-order dissociation rate of monovalent mAb from mAb-HER2 complex | 1.2 |
| | $k_{off}^{bival}$ | 1/hour | First-order dissociation rate of bivalent mAb from mAb-HER2 complex | 0.25 |
| | $t_{1/2,deg}^{mAb}$ | hour | Degradation half-life of unbound, internalized mAb | 4.3 |
| | $C_1$ | dimensionless | Scaling factor for internalization rate of bivalent mAb-bound HER2, where $t_{1/2,int,bival}^{HER2} = 1/C_1 \cdot t_{1/2,int}^{HER2}$ | 32 |
| | $C_2$ | dimensionless | Scaling factor for degradation rate of bivalent mAb-bound HER2, where $t_{1/2,deg,bival}^{HER2} = 1/C_1 \cdot t_{1/2,deg}^{HER2}$ | 9.2 |
| | $C_3$ | dimensionless | Scaling factor for recycling rate of bivalent mAb-bound HER2, where $t_{1/2,rec,bival}^{HER2} = 1/C_3 \cdot t_{1/2,deg}^{HER2}$ | 1 |
| Derived parameters | $t_{1/2,\ rec}^{HER2}$ | hour | Recycling half-life of unbound and monovalent mAb-bound HER2 | 0.55 |
| | $K_0$ | picomole/hour | Zero-order HER2 synthesis rate | 0.00036 |
| Fixed parameters | $f_{m,SS}^{HER2}$ | dimensionless | Fraction of total HER2 expressed on the cell surface at baseline | 0.95 |
| | $t_{1/2,\ growth}^{HER2}$ | hour | *In vitro* KPL4 growth rate (in-house data) | 35 |
| | $N_0$ | nmol/L | Total HER2 concentration at baseline (in-house data) | 0.24 |

Note: A scatter-search parameter optimization algorithm was used, with lower and upper limits applied to each parameter during optimization. Parameters $C_1$, $C_2$ and $C_3$ are used to explore different mechanisms of antibody internalization ($C_1$), degradation ($C_2$), and recycling ($C_3$) rates, where the rates (in nanomole/hour) for each of these processes is faster by a factor of $C_1$, $C_2$ or $C_3$ for the bivalent mAb compared to the monovalent mAb. Additional details regarding parameter estimation results for all model variants can be found in the Supplemental Material.

the mechanism is assumed to involve antibody-induced HER2 clustering, which would not be triggered by administration of a monovalent anti-HER2 antibody (19). Therefore, all model variants explored here assume that HER2 kinetics are the same for the unbound and monovalent antibody-bound states. The base model structure assumes that HER2 synthesis, recycling, and degradation kinetics are also the same for the unbound and bivalent antibody-bound states. Because it is unclear if antibody binding alters HER2 internalization or trafficking rates (18, 20, 21), additional hypotheses were explored where model variants 1, 2, and 3 assume that internalization, degradation, and recycling rates for the anti-HER2/HER2 complexes differ from that of unbound HER2 by a factor of fitted parameters $C_1$, $C_2$, and $C_3$, respectively. Model variants 4 to 7 evaluate model parameterizations that include the remaining combinations of $C_1$, $C_2$, and $C_3$. Each model variant was fitted simultaneously to all monovalent and bivalent antibody *in vitro* data.

Model discrimination analysis was performed by comparing the Akaike Information Criterion (AIC; ref. 22) across all fitted model variants, where a lower AIC indicates a more favorable balance between model parsimony and goodness-of-fit and, thus, a "better" model. Here, $\text{AIC} = 2 \times (-\text{LogLikelihood} + N_p)$, where $N_p$ is the number of fitted model parameters. Matlab SimBiology was used for compartmental model development, where unknown parameters were fitted to *in vitro* data using the Matlab scatter search algorithm (23) and the sensitivity of model simulations to numerical precision of fitted parameter values was evaluated by simulating Gaussian prediction confidence intervals. The SimBiology model file, data used for model calibration, and complete model equations are available in the Supplementary Materials and Methods.

# Results

### HER2 valency does not affect systemic exposure

The effect of anti-HER2 antibody valency on tissue levels of intact and catabolized antibody was analyzed using radiolabeled HER2 bivalent (anti-HER2/HER2), HER2 monovalent (anti-gD/HER2), and nonbinding (anti-gD/gD) antibodies in KPL-4 tumor bearing mice. Mice received either a high or low dose of each HER2 antibody format to account for potential dose-dependent PK and distribution differences. The low-dose cohort received 1 mg/kg anti-gD/HER2 and 0.5 mg/kg anti-HER2/HER2, whereas the high-dose cohort received 10 mg/kg anti-gD/HER2 and 5 mg/kg anti-HER2/HER2. Low- and high-dosed groups were normalized on the basis of the number of anti-HER2 binding sites to maintain comparable stoichiometry versus the target at each dose range.

Systemic exposures in plasma were calculated as $AUC_{0-7d}$ using %ID/mL to dose normalize and facilitate comparison of tracer kinetics across doses. At low doses, $^{125}$I-labeled anti-gD/HER2 and anti-HER2/HER2 exhibited similar systemic exposure with mean $AUC_{(0-7d)}$ values of 5,165 (1 mg/kg anti-gD/HER2) and 4,956 (0.5 mg/kg anti-HER2/HER2) %ID/mL*day (**Fig. 1A**). A 10-fold increase in dose similarly showed no significant difference in systemic exposure with mean $AUC_{(0-7d)}$ values of 4,622 (10 mg/kg anti-gD/HER2) and 4,927 (5 mg/kg anti-HER2/HER2) %ID/mL*day (**Fig. 1A**). Comparison of all HER2-targeting antibodies, regardless of dose, did not show a significant difference in exposure ($P = 0.50$, one-way ANOVA; **Fig. 1A**). All HER2 antibodies demonstrated a decrease in systemic exposure compared with the nonbinding control (anti-gD/gD; $P = 0.002$ to 0.03), likely due to target-mediated drug disposition (TMDD) in tumor bearing mice as seen previously with the

Published OnlineFirst July 12, 2021; DOI: 10.1158/1535-7163.MCT-20-1097



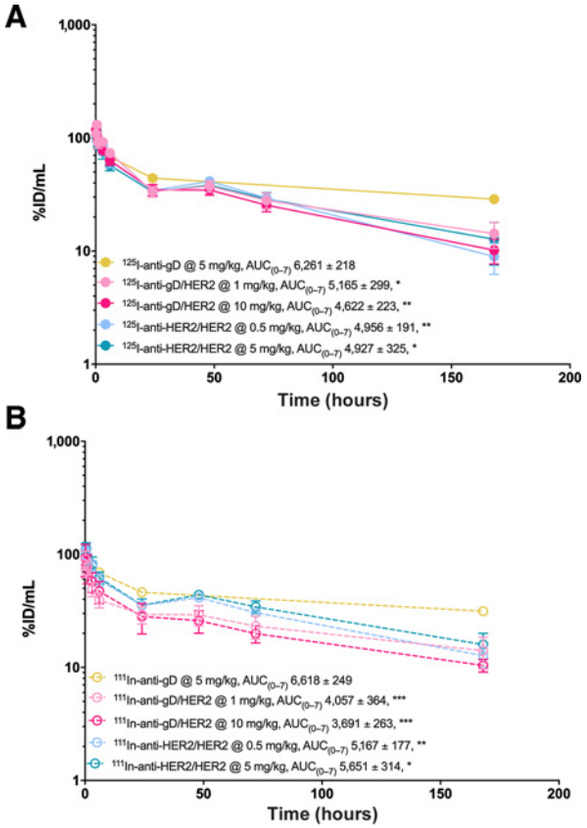


**Figure 1.**

Impact of HER2 targeting antibody valency on dose-normalized systemic (plasma) exposure in KPL-4 tumor bearing mice. SCID.bg mice bearing KPL-4 tumors in mammary fat pads were injected with a single IV bolus of $^{125}$I- and $^{111}$In-labeled monovalent HER2 binding (anti-gD/HER2, 1 or 10 mg/kg), bivalent HER2 binding (anti-HER2/HER2, 0.5 or 5 mg/kg) or nonbinding control (anti-gD/gD, 5 mg/kg) antibodies. Sparse blood samples were collected from 0 to 7 days. Plasma concentrations of $^{125}$I radiolabeled (**A**) and $^{111}$In radiolabeled (**B**) antibodies are represented as %ID/mL. Exposures (AUC ± SEM) were calculated using GraphPad Prism, and significance was determined using a Student *t* test comparing the multiple exposures to anti-gD/gD.

traditional humanized 4D5 bivalent antibody, trastuzumab (**Fig. 1A**; ref. 24). Similar systemic exposure trends were also observed with $^{111}$In-labeled antibodies, but with a larger degree of variability (**Fig. 1B**). Evaluation of whole blood exposure showed similar patterns, suggesting that there was no blood cell partitioning (Supplementary Fig. S1). Additional PK parameters such as $C_{max}$, CL, $V_{ss}$, half-life, and dose-normalized $AUC_{(0-7)}$ were also calculated and found to be similar between HER2-targeting antibodies (Supplementary Table S1).

### HER2 valency does not affect levels of intact antibody in nontarget tissues

Splenic antibody distribution in immunocompromised mice is often nonlinear due to dose-dependent saturation of FcγR, as previously shown (25). At earlier time points splenic distribution of intact ($^{125}$I) antibody (solid bars) is inversely related to dose (**Fig. 2A**), suggesting FcγR saturation. At 6 hours, splenic intact antibody level of the lowest dosed HER2 antibody (0.5 mg/kg, anti-HER2/HER2) was 33.9%ID/g whereas the highest dosed HER2 antibody (10 mg/kg, anti-gD/HER2) was 14.9%ID/g (**Fig. 2A**). However, the splenic distribution of intact antibody across all doses become similar by the 1 day time point, which is approximately the time point in which the dosed antibodies transitioned from distribution phase to elimination phase (**Fig. 2B**). At the final 7-day time point, the nonbinding control antibody (5 mg/kg, anti-gD/gD) had the highest splenic enrichment of 9.6%ID/g compared with the HER2 antibodies (2.4 to 4.1%ID/g, **Fig. 2C**). However, this difference reflects the higher systemic exposure for anti-gD/gD and does not appear to be related to inherent targeting properties (**Figs. 1A** and **2C**). Similar, but lower magnitude differences were observed in all other tissues (heart, liver, kidney, muscle) when comparing anti-gD/gD to both HER2 targeting antibodies (**Fig. 2A–C**). Tissue distribution data for all tissues are summarized in Supplementary Fig. S2.

### HER2 valency does not affect levels of intact antibody in tumor

Throughout the biodistribution study, HER2 targeting valency did not dramatically affect intact antibody levels (including receptor bound and free interstitial pools), whether at high- or low-dose levels. Both anti-gD/HER2 and anti-HER2/HER2 exhibited similar concentrations of intact ($^{125}$I) antibody levels, indicated as solid bars, in tumors across 7 days (**Fig. 2**). Intact HER2-targeting antibody concentrations ranged from 11.8 to 13.4%ID/g at 6 hours (**Fig. 2A**) with a minimal increase to 11.6 to 16.4%ID/g by 24 hours (**Fig. 2B**). At 7 days, the different HER2-targeting antibodies continued to show similar tumor concentration, but at declining levels in a pseudo-state equilibrium with plasma levels (**Fig. 2C**).

Given the high copy number of $\sim 10^6$ HER2 receptors per tumor cell, the absence of apparent dose-dependent competitive inhibition of HER2 antibody distribution in tumor is not surprising. While occasional, significant differences were evident at some time points, consistent trends for intact antibody levels in tumors were observed for all antibodies (**Fig. 2A–C**; Supplementary Table S2). Taken together, the increased valency did not lead to any significant change in tumor concentration of intact antibody over 7 days.

### Increased HER2 valency increases antibody catabolism in tumor

Antibody catabolism ($^{111}$In minus $^{125}$I), indicated as open bars, increased over time for all HER2-targeting antibodies in tumors. At 6 hours, anti-gD/HER2 showed very little tumor catabolism ranging from below the limit of detection to 0.6%ID/g, whereas anti-HER2/HER2 catabolism was up to 10-fold higher, ranging (across two dose levels) from 6.4%ID/g to 7.1%ID/g (**Fig. 2A**). At 1 day, anti-gD/HER2 showed early signs of catabolism ranging from 5.9%ID/g to 13.6%ID/g (**Fig. 2B**) whereas anti-HER2/HER2 had a roughly 2-fold higher catabolism ranging from 20%ID/g to 23.1%ID/g (**Fig. 2B**). By day 7, anti-gD/HER2 showed a further increase in tumor catabolism ranging from 17.7%ID/g to 20.2%ID/g, but was still roughly half that of anti-HER2/HER2 (36.8–47.1%ID/g, **Fig. 2C** and **D**). Low amounts of tumor catabolism were observed for anti-gD/gD at 7 days, but may be attributed to nonspecific (pinocytotic) uptake (3.4%ID/g, **Fig. 2C** and **D**). For all molecules, tissue catabolism outside of the tumor was only observed in clearance organs at relatively low levels, under 10%ID/g (**Figs. 2A–C**). Although increased valency does not affect levels of intact antibody in tumor, an increase in antibody catabolism in tumor was observed with increased valency. Importantly, receptor-mediated antibody internalization and catabolism implies prior receptor engagement.

Published OnlineFirst July 12, 2021; DOI: 10.1158/1535-7163.MCT-20-1097



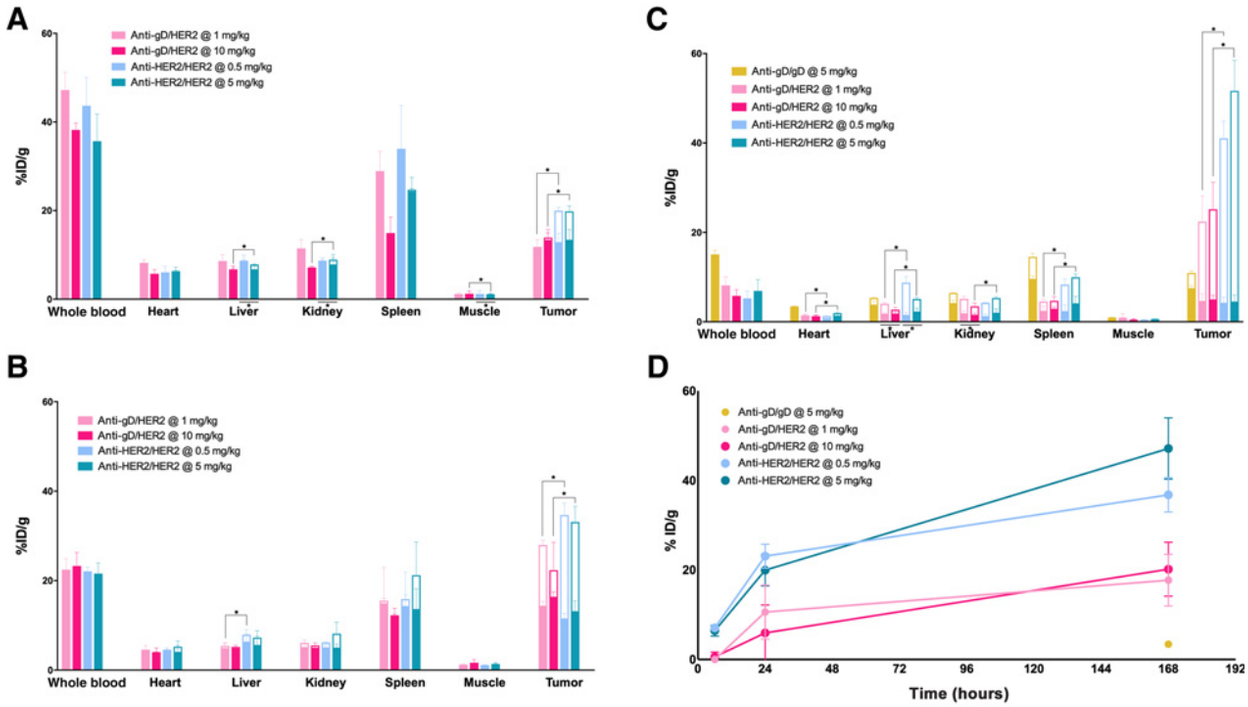


**Figure 2.**

Impact of HER2 targeting antibody valency on tissue distribution and dose-normalized uptake in KPL-4 tumor bearing mice. SCID.bg mice bearing KPL-4 tumors in mammary fat pads were injected with a single IV bolus of $^{125}$I- and $^{111}$In-labeled monovalent HER2 binding (anti-gD/HER2, 1 or 10 mg/kg), bivalent HER2 binding (anti-HER2/HER2, 0.5 or 5 mg/kg) or nonbinding control (anti-gD/gD, 5 mg/kg) antibodies. Tissue enrichment of antibodies is expressed as %ID/g. Intact antibodies (solid bars) were determined from the measurement of $^{125}$I. The amount of catabolized antibody (open bars) is calculated as $^{111}$In-labeled antibody %ID/g minus $^{125}$I-labeled antibody %ID/g (Intact + Catabolized − Intact). Intact antibody distribution and catabolism were measured at 6 hours (**A**), 1 day (**B**), and 7 days (**C**) after dose. Catabolized antibody was measured in tumor over the course of the study (**D**). All graphs show means ± SD error bars for each group ($n = 4$). *P* values were obtained by Student *t* test. Comparisons of amount catabolized between groups were indicated as significant with asterisks over the bars. In addition, comparisons of amount catabolized for low dose versus high dose within valency groups were indicated as significant via lines under the bars. All significant *P* values were reported as $^*P < 0.05$.

### SPECT-CT imaging demonstrates increased tumor distribution and uptake for bivalent compared with monovalent anti-HER2 antibodies

To observe longitudinal tumor uptake, we employed noninvasive SPECT-CT imaging to track tissue levels of intact and catabolized antibodies over time using $^{111}$In. Within the first few hours following intravenous dosing, the pattern of systemic exposure for all antibodies matches the pattern of observed distribution in tumors (**Fig. 3A**). By 24 hours, increased tumor accumulation of radioactive signal was observed for both anti-gD/HER2 and anti-HER2/HER2, but not for anti-gD/gD (**Fig. 3A**). Consistent with the biodistribution data, all anti-HER2 targeting antibodies showed faster whole body radioactivity clearance compared with the nonbinding gD control (Supplementary Fig. S3). Also consistent with the biodistribution data, anti-HER2/HER2 had >2-fold increased tumor uptake compared with anti-gD/HER2 that persisted to 7 days (**Fig. 3B**).

Subsequent analysis of tumors by 3D autoradiography similarly showed higher levels of anti-HER2/HER2 antibodies. Tumor uptake of $^{111}$In-labeled antibodies for anti-gD/gD was 9% ID/g, whereas anti-gD/HER2 was 22.2%ID/g and anti-HER2/HER2 was 61.7%ID/g (**Fig. 3C**). However, at a resolution of ∼250 μm$^3$ intratumoral distribution of anti-HER2/HER2 antibodies throughout the tumor appeared to be heterogeneous, showing isolated regions of higher signal whereas the anti-gD/HER2 tumor showed a more consistent, homogeneous signal throughout the tumor (**Fig. 3C**).

### Increased HER2 valency decreases tumor penetration

To further characterize potential differences in tumor penetration at higher resolution, tumors from the biodistribution study were processed for microscopy. Dosed antibodies that remained intact were detected using immunofluorescence and imaged at the same exposures for comparison with representative images shown in **Fig. 4**. The total dose of antibodies was different for each group, thus precluding direct comparison of signal intensity. However, the overall qualitative intratumoral distribution patterns showed that anti-HER2/HER2 antibodies at both the low (0.5 mg/kg) and high doses (5 mg/kg) had more heterogeneous distribution and therefore lower tumor penetration at 6 hours in comparison to the high-dose anti-gD/HER2 antibody group. A heterogenous intratumoral distribution was also observed for anti-gD/HER2 dosed animals at 1 mg/kg. However, anti-gD/HER2 at the highest dose of 10 mg/kg demonstrated more homogeneous intratumoral distribution and therefore greater tumor penetration, consistent with previous findings that increasing antibody dose can overcome potential epitope barriers in high expression tumor models (26).

### Increased valency increases cellular binding *in vitro*

Using a radioactive cell-based assay, we further investigated the effect of HER2 valency on cell binding, internalization, and catabolism with HER2 bivalent (anti-HER2/HER2), HER2 monovalent (anti-gD/HER2), and nonbinding (anti-gD/gD) antibodies. Cultured

Published OnlineFirst July 12, 2021; DOI: 10.1158/1535-7163.MCT-20-1097



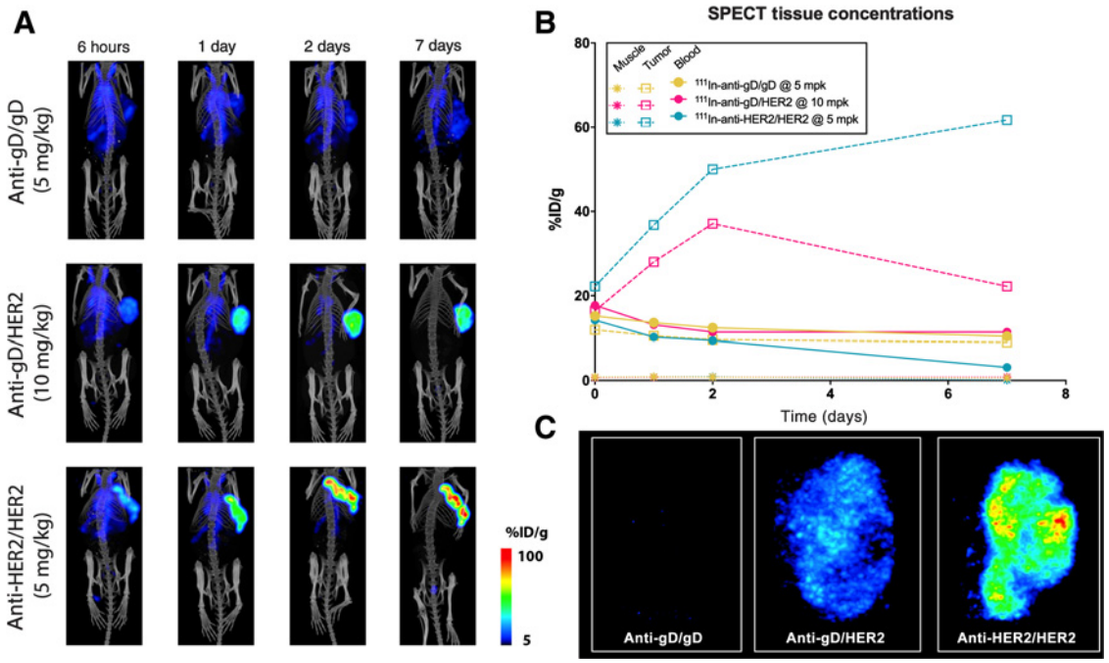


**Figure 3.**

Longitudinal SPECT-CT imaging of nonbinding, monovalent and bivalent HER2 targeting antibodies in KPL-4 tumor-bearing mice. SCID.bg mice bearing KPL-4 tumors in mammary fat pads received $^{111}$In-labeled antibodies, representing distribution of both intact and catabolized antibodies. Mice dosed with 5 mg/kg anti-gD/gD, 10 mg/kg anti-gD/HER2, and 5 mg/kg anti-HER2/HER2 received a single IV bolus of ~700 uCi of $^{111}$In-labeled antibody and imaged at 6 hours and days 1, 2, and 7 using SPECT-CT (**A**). All images were acquired consistently and visualized using VivoQuant software at the same decay-corrected exposures to depict changes in relative accumulation. **B,** 3D tissue ROIs were generated using VQ software and reported as %ID/g. **C,** At 7 days after injection, excised tumors from mice that were subjected to tissue distribution analysis were imaged by 3D-tissue autoradiography for 5 mg/kg anti-gD/gD, 10 mg/kg anti-gD/HER2, and 5 mg/kg anti-HER2/HER2 dosed mice.

KPL-4 cells were incubated with $^{125}$I and $^{111}$In-labeled antibodies, again utilizing the dual tracer approach to distinguish intact from catabolized antibodies.

Intact antibody binding (open circles) was highest for anti-HER2/HER2, with a maximal binding of 22.4% antibody plated (%AP) observed at approximately 12 hours (**Fig. 5C**). In contrast, anti-gD/HER2 showed delayed and reduced binding kinetics with a maximal binding of 14.3%AP at approximately 48 to 72 hours (**Fig. 5B**). Following the trend of increased intact antibody binding, anti-HER2/HER2 also showed increased antibody catabolism (filled circles) with 47%AP compared with anti-gD/HER2 with 12.1%AP accumulated by 72 hours (**Fig. 5B** and **C**). For both the bivalent and monovalent antibodies, the rise in catabolism corresponds with the rise in antibody binding (**Fig. 5B** and **C**). The low binding (0.1%AP) and catabolism (0.02%AP) of the nonbinding antibody (anti-gD/gD) over 72 hours suggests any binding or catabolism due to pinocytosis or nonspecific binding is negligible (Supplementary Fig. S4). Taken together, these data confirm that increased HER2 valency, and therefore apparent affinity, leads to an increase in the magnitude of HER2 target binding and catabolism.

### Compartmental modeling yields insight into mechanisms of *in vitro* binding and uptake

A compartmental modeling approach was used to further elucidate our findings from the radioactive *in vitro* assay. The Base model and seven variants were evaluated and Model Variant 4 (faster internalization and degradation of the bivalent antibody/HER2 complex via parameters $C_1$ and $C_2$, respectively) was found to be optimal based on a low AIC value (AIC = 420) compared with the base model (AIC = 583; **Table 1**; Supplementary Table S3). Model variant 1 (faster internalization of anti-HER2 antibodies) and Model variant 7 (faster internalization, degradation and recycling of anti-HER2 antibodies) both have similarly low AIC values (423), but yielded $C_1$ (and $C_3$ for variant 7) values with high standard errors indicating low numerical precision and potential numerical identifiability issues (see Supplementary Materials and Methods). **Fig. 5B** and **C** show the *in vitro* data for monovalent (anti-gD/HER2) and bivalent (anti-HER2/HER2) antibodies along with the fitted simulations generated by model variant 4 (blue curves). Numerical precision is reflected by the 95% gaussian confidence intervals (shaded regions). Fitted base model simulations are shown as gray curves and demonstrate qualitatively poor agreement with the experimental data. Comparison of the base model fits with those of model variant 4 strongly suggest that there are differences in internalization and potentially in subsequent trafficking rates between the monovalent and bivalent antibodies. The poor fits to data achieved with the base model suggests that the *in vitro* data cannot be explained by differences in valency, and therefore apparent binding affinity, alone. AICs and fitted parameter values for the base model and all variants are listed in Supplementary Table S3. Fitted parameter values of the base model and variant 4 are all within an order of magnitude of assumed/nominal physiologic values (18, 27). Fitted parameter values for model variant 4 are all within an order of magnitude of assumed/nominal physiologic values (18, 27). Fitted variant 4 values of $K_D$ ($K_{D,\text{anti-gD/HER2}}$ = 4.4 nmol/L and $K_{D,\text{anti-HER2/HER2}}$ = 0.6 nmol/L) are close to assay-based values, where measured $K_D$ for the monovalent antibody is 1.5 and 10.5 nmol/L for

Published OnlineFirst July 12, 2021; DOI: 10.1158/1535-7163.MCT-20-1097



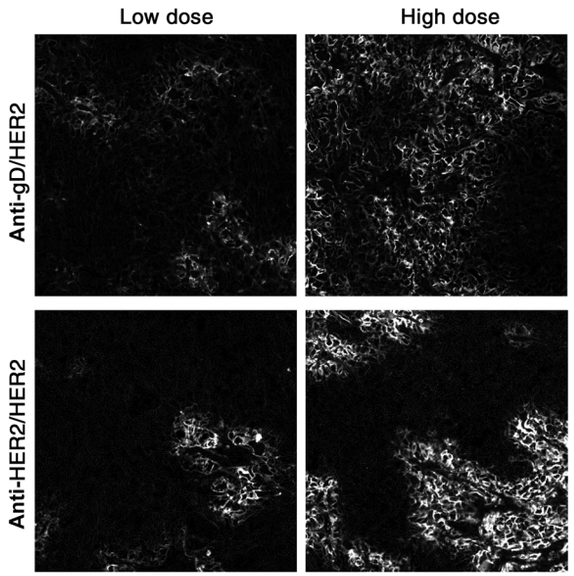


**Figure 4.**

Immunofluorescence imaging depicts tumor penetration of monovalent and bivalent HER2 targeting antibodies in KPL-4 tumors at 6 hours. SCID.bg mice bearing KPL-4 tumors in mammary fat pads received a single IV bolus of monovalent HER2 (anti-gD/HER2, 1 or 10 mg/kg) or bivalent HER2 (anti-HER2/HER2, 0.5 or 5 mg/kg). At 6 hours, tumors were excised and prepared for tissue immunolabeling with fluorescent detection. Sections were imaged using similar exposure levels and representative images shown.

cell-based and SPR-based estimates and measured $K_D$ for the bivalent antibody is 0.5 and 0.8 nmol/L for cell-based and SPR-based estimates (in-house data).

## Discussion

We sought to determine the impact of antibody valency on tumor distribution and catabolism in a preclinical model of HER2+ breast cancer. Bivalency is a key functional attribute of most full-length IgG antibodies (both endogenous and engineered), yet we are unaware of any previous study in which the targeting abilities of monovalent and bivalent full-length antibodies were directly compared. The impact of valency and consequent apparent affinity (conferred by avidity) in the success of antibody targeting can be difficult to evaluate, although its importance has been widely discussed in the context of the binding site barrier concept (28). Even direct comparison of tumor targeting data for Fab and F(ab')$_2$ fragments is difficult to interpret due to size-driven differences in renal filtration rates (and hence systemic exposures; ref. 29). Our experimental design addressed these limitations by ensuring that all variables, for example, Fc binding, molecular size/shape, other than binding valency remained similar between two full-length HER2-binding IgGs, a monovalent (anti-gD/HER2) and bivalent (anti-HER2/HER2), with a third nonbinding antibody (anti-gD/gD) serving as a control for nonspecific distribution and pinocytosis driven uptake.

Similar exposures between monovalent and bivalent antibodies confirm that differences in pharmacokinetics could not explain the discrepancy in tumor catabolism (**Fig. 1**). These findings have broad implications for anticancer therapy with biologics, particularly for modalities in which the mechanism of action relies on the molecular fate of the antibody. For instance, the development of many ADCs against internalizing targets has aimed to achieve intracellular delivery of cytotoxic payloads, and the data herein suggest that bivalent antibodies may allow more efficient intracellular delivery of drug payloads by virtue of enhanced internalization (30). However, other factors such as how avidity and affinity collectively affect tumor penetration must also be considered when targeting solid tumors. In contrast to ADCs, TDBs must remain extracellular and intact to achieve bridging of target cancer cells with T cells. Therefore, the lower degree of internalization in addition to the higher degree of tumor penetration that we observe for anti-gD/HER2 suggest that monovalent formats should be better equipped for T-cell engagement (4). Caution must be exercised, however, because these findings for HER2 may not necessarily extend to other cancer targets.

We demonstrated that anti-HER2/HER2 showed heterogeneous uptake in a HER2 expressing model (**Fig. 4**), consistent with previous work (31–34). Importantly, far more homogeneous tumor penetration was observed for anti-gD/HER2 than for anti-HER2/HER2 in a dose-dependent manner, suggesting that the bivalent binding can also significantly contribute to the binding site barrier. This may be attributed to one or more factors: (i) bivalency increases the probability of a binding event, (ii) bivalency enhances or promotes receptor internalization via crosslinking of receptors, and/or (iii) bivalency tends to result in greater perivascular receptor occupancy. Some studies have previously concluded that HER2 internalization is passive and is unaffected by trastuzumab binding (18) whereas others have concluded that trastuzumab binding can induce sustained internalization of HER2 (16). Furthermore, others have demonstrated that incubation with trastuzumab can depress the cell surface HER2 pool, possibly representing a resistance mechanism to anti-HER2 therapies (35). However, it has become generally accepted in the field that if HER2 down-modulation does occur upon interaction with trastuzumab, it is transient. These suggest that HER2 cell surface levels remain fairly constant. These seemingly conflicting views warrant further characterization of the extent to which HER2 internalization kinetics may be affected by engagement with anti-HER2 antibody therapeutics.

The trend of higher catabolism for bivalent anti-HER2/HER2 compared with monovalent anti-gD/HER2 *in vivo* by both invasive tissue harvesting (**Fig. 2**) and noninvasive SPECT-CT imaging (**Fig. 3**) was consistent with the *in vitro* data. *In vitro*, tumor cells were exposed to anti-HER2/HER2 concentrations that were similar in magnitude to $K_D$ ($K_D$-bivalent $\approx$ 0.5 nmol/L); however, anti-gD/HER2 concentrations were approximately 10$\times$ below $K_D$ (where $K_D$-monovalent $\approx$ 5 nmol/L; Supplementary Fig. S4D). In these studies, antibody concentrations 10$\times$ below $K_D$ resulted in significantly lower receptor occupancy (RO) compared with the bivalent antibody, which dramatically exaggerated the observed *in vitro* differences in binding and catabolism. This is very different compared with the *in vivo* study studies where all doses yielded antibody tissue concentrations in the μmol/L range, well above the $K_D$ for both HER2 targeting antibodies, resulting in presumably high RO, internalization and subsequent residualization for both the monovalent and bivalent antibodies. Subsequently, the *in vivo* study showed that both HER2 targeting antibodies had considerable uptake, reflecting the higher RO in both cases. Observed differences in uptake between the monovalent and bivalent antibody likely reflected the differences in $K_D$ and possibly increased internalization rates for the bivalent antibody.

Compartmental modeling yielded insights into anti-HER2 antibody binding and trafficking mechanisms associated with the

Published OnlineFirst July 12, 2021; DOI: 10.1158/1535-7163.MCT-20-1097



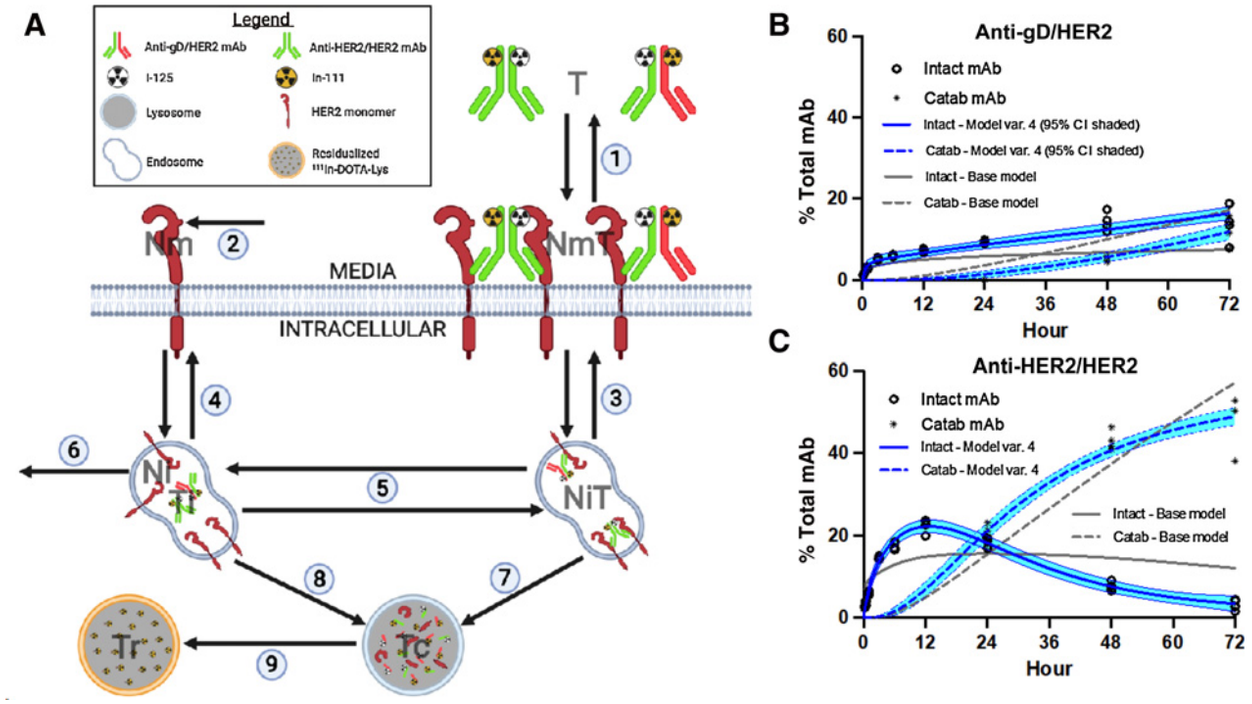


**Figure 5.**

Compartmental model structure and fits. **A,** High-level schematic of a compartmental model for *in vitro* anti-gD/HER2 and anti-HER2/HER2 binding and trafficking kinetics. The following reactions and molecular species (in parenthesis) are explicitly represented in the model: (1) forward and reverse binding of free antibody in media (**T**) to free cell-surface HER2 (**Nm**), (2) synthesis of free cell-surface HER2 (**Nm**), (3) internalization of the mAb/HER2 complex at the cell surface (**NmT**) and recycling of endosomal mAb/HER2 complex (**NiT**) back to the cell surface, (4) internalization of free HER2 at the cell surface (**Nm**) and recycling of free endosomal HER2 (**Ni**) back to the cell surface, (5) forward and reverse binding of free endosomal antibody (**Ti**) to free endosomal HER2 (**Ni**), (6) degradation of free endosomal HER2 (**Ni**), (7) degradation of endosomal mAb/HER2 complex (**NiT**), (8) degradation of free endosomal mAb (**Ti**), and (9) time delay between late endosome/lysosome and residualized $^{111}$In-mAb compartments (**Tc**) and residualization of $^{111}$In-labeled catabolites (**Tr**). Supplementary Fig. S5 lists the equations associated with each of these reactions. The Matlab/Simbiology model and data files, and complete model equations can also be found in the Supplementary Materials and Methods. Illustration created with BioRender.com. **B,** Observed *in vitro* uptake of monovalent anti-gDHER2 mAbs in KPL4 cells. Model variant 4 (where bivalent mAb/HER2 complex is internalized and degraded at a faster rate compared with unbound HER2 and monovalent mAb/HER2 complex) fitted to data along with 95% confidence interval is shown as blue curves and shaded region; the base model (internalization/trafficking kinetics are the same for unbound HER2, monovalent mAb/HER2 complex, and bivalent mAb/HER2 complex) fitted to data is shown as gray curves. **C,** Observed *in vitro* uptake of bivalent anti-HER2/HER2 mAbs in KPL4 cells. Model variant 4 fitted to data along with 95% confidence interval is shown as blue curves and shaded region; the base model fitted to data is shown as gray curves. Model was simultaneously fitted to all monovalent and bivalent mAb data.

*in vitro* KPL4 antibody uptake data. Comparison of the base model and variant 4 fits shown in **Fig. 5B** and **C** suggest that significant differences between monovalent and bivalent antibody/HER2 complex internalization and potentially other trafficking rates are required to explain the increased catabolism we observe for the bivalent antibodies in comparison to the monovalent antibodies (gray and blue curves). The greatest improvement in model fits is achieved by invoking the hypothesis associated with model variant 4, which assumes the rates of anti-HER2 antibody internalization and degradation within endosomes are higher for the bivalent antibody than for the monovalent antibody. Additional studies would be required to better understand differences between monovalent and bivalent anti-HER2 antibody trafficking kinetics; however our preliminary analysis suggests that the observed *in vitro* data cannot be explained by differences in valency (and subsequent binding affinity) alone.

Supplementary Fig. S4 provides a mechanistic explanation of each kinetic phase of the *in vitro* data, where the intact monovalent antibody (Supplementary Fig. S4A) rapidly (1–2 hours) reaches binding equilibrium with cell-surface HER2 due to its lower affinity and faster compartmental model based $k_{off}$ ($\approx$1 hour$^{-1}$) and accumulates within the intracellular (endosomal) space until an apparent steady-state is reached, at approximately 48 hours. The free antibody concentration is expected to be approximately constant over the course of the study due to the relatively low affinity of the monovalent antibody compared with HER2 concentration (Supplementary Fig. S4D). Accumulation of catabolized monovalent antibody within the intracellular (lysosomal) space is not apparent until approximately >20 hours, suggesting a time delay in this process, and continues to increase linearly until the end of the study at 72 hours. This time delay represents the time required for radiolabeled antibodies to be trafficked from early to late endosomes/lysosomes and to subsequently be catabolized. It is included in the model between compartments $T_c$ and $T_r$ (**Fig. 5A**), where the $T_c$ compartment represents the late endosomal stage at which antibody catabolism is just beginning. Intact bivalent antibody (Supplementary Fig. S4B) reaches binding equilibrium relatively slowly (approx. 10 hours) with cell-surface HER2 due to its higher affinity and slower compartmental model based $k_{off}$ ($\approx$ 0.3 hour$^{-1}$). On the basis of the compartmental modeling, we speculate that accumulation within the intracellular (endosomal) space is quickly countered by apparent

Published OnlineFirst July 12, 2021; DOI: 10.1158/1535-7163.MCT-20-1097



depletion of antibody from the media, due to relatively high affinity of the bivalent antibody compared with HER2 concentration (Supplementary Fig. S4D). Accumulation of catabolized bivalent antibody within the intracellular (lysosomal) space is not apparent until approximately >20 hours, again suggesting a time delay in this process. The rate of accumulation of bivalent antibody catabolites slows as antibody is depleted from media.

In conclusion, we have demonstrated how valency affects *in vivo* distribution, including tumor-specific targeting and internalization, by comparing monovalent (anti-gD/HER2) and bivalent (anti-HER2/HER2) HER2-targeting antibodies in a xenograft model of breast cancer. *In vitro*, the bivalent antibody exhibited higher levels of binding and catabolism compared with the monovalent antibody that cannot be explained by increased valency and subsequent higher apparent binding affinity (conferred by avidity) alone. *In vivo*, higher levels of tumor cell catabolism were also observed for the bivalent compared with the monovalent antibody despite similar blood exposures and similar concentrations of intact antibody in most tissues. These findings may inform multiple antibody therapeutic modalities including T-cell-redirecting therapies (e.g., TDBs) as well as drug delivery strategies relying upon receptor internalization (e.g., ADCs).

## Authors' Disclosures

D. Mandikian reports employment with Genentech Inc., and ownership of Roche stock. L.N. Sermeño reports employment with Genentech, Inc. J. Ho reports employment with Genentech, Inc., and ownership of Roche stock. C. Spiess reports employment with Genentech, Inc., and ownership of Roche stock. A.V. Kamath reports employment with Genentech, Inc., and ownership of Roche stock. G.Z. Ferl reports employment with Genentech, Inc., and ownership of Roche stock. C. Boswell reports employment with Genentech, Inc., and ownership of Roche stock. No disclosures were reported by the other authors.

## Authors' Contributions

**M.K. Ramos:** Conceptualization, data curation, software, formal analysis, validation, investigation, methodology, writing–original draft, writing–review and editing. **D. Mandikian:** Conceptualization, resources, data curation, formal analysis, investigation, writing–original draft, writing–review and editing. **L.N. Sermeño:** Data curation, software, formal analysis, methodology, writing–review and editing. **A. King:** Data curation, formal analysis, validation, investigation, writing–review and editing. **A.T. Dent:** Data curation, formal analysis, investigation, writing–review and editing. **J. Ho:** Data curation, investigation, methodology, writing-review and editing. **S. Ulufatu:** Data curation, validation, methodology, writing–review and editing. **T.N. Lombana:** Resources, data curation, supervision, validation, investigation, writing–review and editing. **C. Spiess:** Conceptualization, resources, supervision, validation, methodology, writing–original draft, writing–review and editing. **M.A.T. Go:** Resources, investigation, methodology, writing–review and editing. **S. Yu:** Conceptualization, supervision, methodology, writing–review and editing. **A.V. Kamath:** Conceptualization, resources, supervision, funding acquisition, project administration, writing–review and editing. **G.Z. Ferl:** Conceptualization, data curation, software, formal analysis, validation, investigation, methodology, writing–original draft, writing–review and editing. **C.A. Boswell:** Conceptualization, resources, data curation, supervision, funding acquisition, validation, methodology, writing–original draft, writing–review and editing.

## Acknowledgments

The authors would like to thank Meric Ovacik, Saroja Ramanujan, Iraj Hosseini, Isabel Figueroa, and Simon Williams for helpful discussions and Nicole Valle, Cynthia Young, Elizabeth Torres, Shannon Liu, Konnie Urban, Christopher Stevenson, Ka Man Li, and Shannon Stainton for technical support.

The costs of publication of this article were defrayed in part by the payment of page charges. This article must therefore be hereby marked *advertisement* in accordance with 18 U.S.C. Section 1734 solely to indicate this fact.

Received December 17, 2020; revised April 19, 2021; accepted June 29, 2021; published first July 12, 2021.

## References

1. Labrijn AF, Janmaat ML, Reichert JM, Parren P. Bispecific antibodies: a mechanistic review of the pipeline. Nat Rev Drug Discov 2019;18:585–608.
2. Spiess C, Zhai Q, Carter PJ. Alternative molecular formats and therapeutic applications for bispecific antibodies. Mol Immunol 2015;67(2 Pt A):95–106.
3. Li J, Stagg NJ, Johnston J, Harris MJ, Menzies SA, DiCara D, et al. Membrane-Proximal epitope facilitates efficient T cell synapse formation by anti-FcRH5/CD3 and is a requirement for myeloma cell killing. Cancer Cell 2017;31:383–95.
4. Mandikian D, Takahashi N, Lo AA, Li J, Eastham-Anderson J, Slaga D, et al. Relative target affinities of T-cell-dependent bispecific antibodies determine biodistribution in a solid tumor mouse model. Mol Cancer Ther 2018;17:776–85.
5. Smith EJ, Olson K, Haber LJ, Varghese B, Duramad P, Tustian AD, et al. A novel, native-format bispecific antibody triggering T-cell killing of B-cells is robustly active in mouse tumor models and cynomolgus monkeys. Sci Rep 2015;5:17943.
6. Kantarjian H, Stein A, Gokbuget N, Fielding AK, Schuh AC, Ribera JM, et al. Blinatumomab versus chemotherapy for advanced acute lymphoblastic leukemia. N Engl J Med 2017;376:836–47.
7. Junttila TT, Li J, Johnston J, Hristopoulos M, Clark R, Ellerman D, et al. Antitumor efficacy of a bispecific antibody that targets HER2 and activates T cells. Cancer Res 2014;74:5561–71.
8. https://clinicaltrials.gov. A phase I study of BTRC4017A in participants with locally advanced or metastatic HER2-expressing cancers. Clinical Trial Identifier NCT03448042.
9. Minchinton AI, Tannock IF. Drug penetration in solid tumours. Nat Rev Cancer 2006;6:583–92.
10. Baker JH, Lindquist KE, Huxham LA, Kyle AH, Sy JT, Minchinton AI. Direct visualization of heterogeneous extravascular distribution of trastuzumab in human epidermal growth factor receptor type 2 overexpressing xenografts. Clin Cancer Res 2008;14:2171–9.
11. Bien-Ly N, Yu YJ, Bumbaca D, Elstrott J, Boswell CA, Zhang Y, et al. Transferrin receptor (TfR) trafficking determines brain uptake of TfR antibody affinity variants. J Exp Med 2014;211:233–44.
12. Carter P, Presta L, Gorman CM, Ridgway JB, Henner D, Wong WL, et al. Humanization of an anti-p185HER2 antibody for human cancer therapy. Proc Natl Acad Sci U S A 1992;89:4285–9.
13. Atwell S, Ridgway JB, Wells JA, Carter P. Stable heterodimers from remodeling the domain interface of a homodimer using a phage display library. J Mol Biol 1997;270:26–35.
14. Ridgway JB, Presta LG, Carter P. 'Knobs-into-holes' engineering of antibody CH3 domains for heavy chain heterodimerization. Protein Eng 1996;9:617–21.
15. Boswell CA, Marik J, Elowson MJ, Reyes NA, Ulufatu S, Bumbaca D, et al. Enhanced tumor retention of a radiohalogen label for site-specific modification of antibodies. J Med Chem 2013;56:9418–26.
16. Fehling-Kaschek M, Peckys DB, Kaschek D, Timmer J, Jonge N. Mathematical modeling of drug-induced receptor internalization in the HER2-positive SKBR3 breast cancer cell-line. Sci Rep 2019;9:12709.
17. Hendriks BS, Opresko LK, Wiley HS, Lauffenburger D. Coregulation of epidermal growth factor receptor/human epidermal growth factor receptor 2 (HER2) levels and locations: quantitative analysis of HER2 overexpression effects. Cancer Res 2003;63:1130–7.
18. Austin CD, De Maziere AM, Pisacane PI, van Dijk SM, Eigenbrot C, Sliwkowski MX, et al. Endocytosis and sorting of ErbB2 and the site of action of cancer therapeutics trastuzumab and geldanamycin. Mol Biol Cell 2004;15:5268–82.
19. Bertelsen V, Stang E. The mysterious ways of ErbB2/HER2 trafficking. Membranes (Basel) 2014;4:424–46.
20. Press MF, Lenz HJEGFR., HER2 and VEGF pathways: validated targets for cancer treatment. Drugs 2007;67:2045–75.

21. Rudnick SI, Lou J, Shaller CC, Tang Y, Klein-Szanto AJ, Weiner LM, et al. Influence of affinity and antigen internalization on the uptake and penetration of Anti-HER2 antibodies in solid tumors. Cancer Res 2011;71:2250–9.
22. Akaike H. A new look at the statistical model identification. IEEE Trans Autom Control 1974;19:716–23.
23. Gabor A, Banga JR. Robust and efficient parameter estimation in dynamic models of biological systems. BMC Syst Biol 2015;9:74.
24. Bernadou G, Campone M, Merlin JL, Gouilleux-Gruart V, Bachelot T, Lokiec F, et al. Influence of tumour burden on trastuzumab pharmacokinetics in HER2 positive non-metastatic breast cancer. Br J Clin Pharmacol 2016;81:941–8.
25. Sharma SK, Chow A, Monette S, Vivier D, Pourat J, Edwards KJ, et al. Fc-mediated anomalous biodistribution of therapeutic antibodies in immunodeficient mouse models. Cancer Res 2018;78:1820–32.
26. Cilliers C, Menezes B, Nessler I, Linderman J, Thurber GM. Improved tumor penetration and single-cell targeting of antibody-drug conjugates increases anticancer efficacy and host survival. Cancer Res 2018;78:758–68.
27. Slaga D, Ellerman D, Lombana TN, Vij R, Li J, Hristopoulos M, et al. Avidity-based binding to HER2 results in selective killing of HER2-overexpressing cells by anti-HER2/CD3. Sci Transl Med 2018;10:eaat5775.
28. Rudnick SI, Adams GP. Affinity and avidity in antibody-based tumor targeting. Cancer Biother Radiopharm 2009;24:155–61.
29. Covell DG, Barbet J, Holton OD, Black CD, Parker RJ, Weinstein JN. Pharmacokinetics of monoclonal immunoglobulin G1, F(ab')2, and Fab' in mice. Cancer Res 1986;46:3969–78.
30. Prabhu S, Boswell CA, Leipold D, Khawli LA, Li D, Lu D, et al. Antibody delivery of drugs and radionuclides: factors influencing clinical pharmacology. Ther Deliv 2011;2:769–91.
31. Fujimori K, Covell DG, Fletcher JE, Weinstein JN. A modeling analysis of monoclonal antibody percolation through tumors: a binding-site barrier. J Nucl Med 1990;31:1191–8.
32. Juweid M, Neumann R, Paik C, Perez-Bacete MJ, Sato J, van Osdol W, et al. Micropharmacology of monoclonal antibodies in solid tumors: direct experimental evidence for a binding site barrier. Cancer Res 1992;52:5144–53.
33. van Osdol W, Fujimori K, Weinstein JN. An analysis of monoclonal antibody distribution in microscopic tumor nodules: consequences of a "binding site barrier". Cancer Res 1991;51:4776–84.
34. Weinstein JN, van Osdol W. The macroscopic and microscopic pharmacology of monoclonal antibodies. Int J Immunopharmacol 1992;14:457–63.
35. Pereira PMR, Sharma SK, Carter LM, Edwards KJ, Pourat J, Ragupathi A, et al. Caveolin-1 mediates cellular distribution of HER2 and affects trastuzumab binding and therapeutic efficacy. Nat Commun 2018;9:5137.

Published OnlineFirst July 12, 2021; DOI: 10.1158/1535-7163.MCT-20-1097



Molecular Cancer Therapeutics

# Valency of HER2 Targeting Antibodies Influences Tumor Cell Internalization and Penetration

Madeleine K. Ramos, Danielle Mandikian, Lauren N. Sermeño, et al.

*Mol Cancer Ther* 2021;20:1956-1965. Published OnlineFirst July 12, 2021.